PERGAMON

International Journal of Heat and Mass Transfer 42 (1999) 165–179

International Journal of HEAT and MASS TRANSFER

Air–water mass transfer of organics from shallow ponds under laminar recirculation

Ildefonso Cuesta[a], F. X. Grau[a], Francesc Giralt[b,*], Yoram Cohen[c]

[a] *Departament d'Enginyeria Mecánica*

[b] *Departament d'Enginyeria Química, Universitat Rovira i Virgili, Escola Técnia Superior d'Enginyeria Química, Carretera de Salou, s/n, 43006 Tarragona, Spain*

[c] *Department of Chemical Engineering, School of Engineering and Applied Science, University of California at Los Angeles, U.S.A.*

Received 3 November 1997; in final form 6 March 1998

Abstract

Air–water mass transfer of organics from shallow ponds under the influence of weak wind stress on the water surface is studied numerically using a two-dimensional model. The flow field in the pond is investigated using a computational code, based on a second order finite volume approximation, which is used to numerically solve the momentum, mass and continuity conservation equations. Solutions are presented for pond aspect-ratios (length to height) ranging from 1 to 10, Reynolds numbers, based on pond depth, between 16 and 1620, and Schmidt numbers from 667 to 2020. The results show that the water phase flow field is strongly dependent on the wind-induced surface velocity and the aspect ratio of the pond. Based on the numerical study, the liquid-side mass transfer coefficient is correlated with the Reynolds number (Re_L), pond aspect ratio (AR) and the Schmidt number (Sc). Deviations from the simple penetration model increase with increasing pond aspect ratio and decreasing Reynolds number.

Nomenclature

AR pond aspect ratio, L/H
C_w concentration [mol m^{-3}]
C_{wb} well-mixed bulk concentration [mol m^{-3}]
C_{wi} local interface concentration [mol m^{-3}]
D molecular mass diffusivity [m^2 s^{-1}]
g gravitational acceleration [ms^{-2}]
H depth of the pond [m]
k_L liquid-side mass transfer coefficient [m s^{-1}]
k_g gas-side mass transfer coefficient [m s^{-1}]
L length of the pond [m]
n unit vector normal to the wall
P Pressure normalized with respect to ρU_s^2
Re_H Reynolds number, UH/v
Re_L Reynolds number, UL/v
Sc Schmidt number v/D
Sh_L Sherwood number, $k_L L/D$
Sh_H Sherwood number, $k_H H/D$
t time normalized with respect to H/U_s
$\mathbf{u}_i$ velocity vector normalized with respect to U_s
U_s free surface velocity [m s^{-1}]
U_{10} wind velocity at 10 m [m s^{-1}]
x_i position vector normalized with respect to H
x, y, z, Cartesian coordinates [m].

Greek letters
δ_c concentration boundary layer thickness [m]
v kinematic viscosity [m^2 s^{-1}]
ρ density [kg m^{-3}].

Superscripts and subscripts
– surface averaged quantity
o initial value.

1. Introduction

Mass transfer rates of volatile organics across natural air–water interfaces plays an important role in numerous

* Corresponding author. Tel.: 00 34 977 558201; fax: 0034 997 558205; e-mail: fgiralt@etseq.urv.es

0017–9310/98 $19.00
PII: S0017–9310(98)00116–1

industrial, geophysical, agricultural and environmental processes. For example in natural and man-made water bodies, knowledge of water–air exchange of chemicals is crucial to understanding multimedia chemical transport and associated potential chemical exposure of human and other ecological receptors [1–3]. The resistance to mass transfer for air–water chemical mass exchange is typically described by the conventional Lewis–Whitman two-film resistance theory which makes use of liquid-side (k_L) and gas-side (k_g) mass transfer coefficients [4]. It is noted that for non-active volatile and sparingly water soluble organics which have a high Henry's law constant, the resistance to mass transfer is generally mostly in the water phase. Thus knowledge of k_L for such chemicals is most important to quantify their water–air chemical exchange rates.

While much research has been done to quantify the rates of chemical mass transfer across the air–water interface, as recently pointed out by Peng et al. [5] most previous studies have focused on situations where the water phase is relatively well-mixed, due to either natural convective currents or wind-induced mixing. The existing theories and correlations for the liquid-side mass transfer coefficient typically apply to turbulent conditions in the water phase [1–3, 6–11]. These approaches do not apply, however, when the wind stress on the water surface and natural convective currents are weak enough and the hydrodynamic conditions are essentially laminar. Such conditions may arise, for example, during calm conditions or when the water bodies are sheltered from the wind and in water bodies of small fetch (e.g., small water reservoirs and holding ponds). In order to evaluate the rate of mass transfer in water bodies where wind-induced water circulation is weak, one has to evaluate the complete hydrodynamics in the water phase and the concentration distribution resulting from chemical transfer through air–water interface.

It has been suggested that correlations for k_L should distinguish three regions depending on wind velocity: (a) the region up to 3 m s^{-1} where the effect of the wind induced current is weak and the water surface is aerodynamically smooth; (b) the region from 3 to 10 m s^{-1} where significant wave action and turbulent wind-induced drift current exist; and (c) above 10 m s^{-1} where wave breaking may occur [3]. Under turbulent conditions mass transfer in the liquid-side is dominated by surface renewal [12, 13]. However, under laminar conditions the liquid-side resistance to mass transfer across the air–water interface is dominated by the concentration boundary layer rather than surface renewal [14]. It is also noted that in small water of short fetch and at the low wind speeds speed regime, a situation of interest in this work, the liquid-side mass transfer coefficients is also likely to be affected by the water body geometry.

In recent years a number of investigators have presented numerical studies of the hydrodynamics [15–19] and sediment–liquid mass transfer [20] in cavities under laminar conditions. For example, the study of Kumagai [17] suggests that the problem of circulation in a cavity, induced by a top lid moving at a constant speed, is suitable for the study of wind-driven circulation because the governing equations are of similar type, provided that the surface is smooth. In the environment, such a conditions is expected for calm winds and water bodies with a relatively short fetch. The circulation in a cavity, induced by a constant uniform surface stress, was studied by Bye [15] and O'Brien [16] for length/depth ratios ranging from 1/3:8 and Reynolds numbers (based on cavity depth) less than 400. These studies demonstrated that a steady-state solution exists and that the shapes and number of vortices strongly depend on the cavity aspect ratio. Simulations at one to two orders of magnitude higher Reynolds numbers were presented by Kumagai [17], Gatski et al. [18] and Neary and Stephanoff [19] suggesting that, as inertial effects become more dominant, significant circulation exists at the downstream end of the cavity. These authors also noted various instabilities which become pronounced with increasing Reynolds number and cavity aspect ratio.

In shallow water bodies, such as small water reservoirs, water impoundments or ponds, which are the focus of this study, the topology of the flow is expected to be affected by the geometry of the water body, i.e., depth and location and configuration of the containing walls [17–19]. Thus the geometry of the pond will also affect mass transfer at both the air–water and sediment–water interfaces. For example, Chang et al. [20] demonstrated, via numerical simulations and experimental data, the effect of length/depth aspect ratio ranging from 0.1 to 10 on wall–liquid mass transfer in cavities subjected to external laminar flow. Earlier experimental studies by Thibodeaux and Baker [21] also indicated that the sediment–water mass transfer coefficient, in a small wind-water tank, subjected to tangential air overflow, was affected by the aspect ratio.

The present work extends previous studies by evaluating the effect of the geometry and Reynolds number on the flow field, under isothermal conditions, and the resulting influence on the rate of mass transfer across the air–water interface. The focus of this study is on chemical mass transfer, across a smooth water–air interface which is set in motion by calm winds setting water circulation in the laminar regime. Knowledge of the local mass transfer coefficient, as a function of position along the pond, would be useful in assessing the average chemical flux under calm conditions. Moreover, information regarding the concentration field would help in designing appropriate sampling strategies.

The present approach considers the numerical study of a two-dimensional cavity with a lid-driven flow to simulate the effect of a weak wind-driven current in a shallow water pond. Three ponds with aspect ratios

(depth : length) of 1 : 1, 4 : 1 and 10 : 1 were studied with a lid speed of up to 0.003 ms^{-1}. Such a low lid speed was selected to simulate nearly calm conditions. Finally, a range of 667–2020 was selected for the Schmidt number to cover a range of organic chemicals which are of interest for their potential environmental impact when evaporating from bodies of water circulating in ponds under laminar conditions.

2. Model description and governing equations

The present analysis is simplified by considering two-dimensional flow of water contained in a rectangular basin of depth, H, and length, L, as illustrated in Fig. 1. The walls in the traverse direction are located sufficiently apart from each other and both H and L are large enough to neglect surface tension effects. Three different geometries were studied, $L = 0.6$, 2.4 and 6 m, with the height of the pond maintained constant at $H = 0.6$ m. These three configurations have aspect ratios $AR = L/H = 1$,4 and 10, respectively.

The unsteady, incompressible flow of water in the pond is governed by the continuity equation

$$\frac{\partial \mathbf{u}_i}{\partial x_i} = 0 \tag{1}$$

and the Navier–Stokes equations, which can be written in non-dimensional form as

$$\frac{\partial \mathbf{u}_i}{\partial t} + \frac{\partial \mathbf{u}_j \mathbf{u}_i}{\partial x_j} = -\frac{\partial P}{\partial x_i} + \frac{1}{Re_H}\frac{\partial^2 \mathbf{u}_i}{\partial x_j \partial x_j} \tag{2}$$

where the gravity term has been included in the pressure term.

The evolution of the concentration field is governed by the mass transport equation, written in a non-dimensional form as

$$\frac{\partial \overline{C_w}}{\partial t} + \frac{\partial \mathbf{u}_i \overline{C_w}}{\partial x_i} = \frac{1}{Re_H Sc}\frac{\partial^2 \overline{C_w}}{\partial x_j \partial x_j} \tag{3}$$

where $\overline{C_w}$ is the dimensionless chemical concentration normalized with respect to the initial concentration in the pond, C_{wo}, at the initial time t_o.

The boundary and initial conditions are defined as follows. At the free surface, $y = H$, the water velocity at the interface is assumed to be constant and it is approximated from $U_s = 0.03 \cdot U_{10}$, where U_{10} is the wind velocity [22]. The present calculations cover the range of $3 \times 10^{-5} \leqslant U_s \leqslant 3 \times 10^{-3}$ m s^{-1} ($10^{-3} \leqslant U_{10} \leqslant 10^{-1}$ m s^{-1}), to assure that the simulations are in the range of wind speeds that correspond to a smooth free surface. At this free boundary, the solute concentration is taken as zero, i.e., the mass transfer process at the interface is assumed to be dominated by the water-side resistance. At the vertical and the bottom walls the non-slip boundary condition leads to $\mathbf{u}_i = 0$. The condition of no-flux at the solid boundaries implies that $\partial \bar{C}_w/\partial \mathbf{n} = 0$ where $\mathbf{n}$ is the unit vector normal to the wall considered. Finally, when solving equation (2), the fluid is assumed to be initially at rest, $(\mathbf{u}_i)_{t=0} = 0$, and when solving equation (3) the initial concentration is taken to be uniform $(\bar{C}_w)_{t=0} = 1$ inside the cavity. The dimensional interfacial local mass flux, from the water side, can be calculated from

$$k_L(C_{wb} - C_{wi}) = -D\left.\frac{\partial C_w}{\partial y}\right|_{y=0} \tag{4}$$

where C_{wb} and C_{wi} are the well-mixed bulk and local

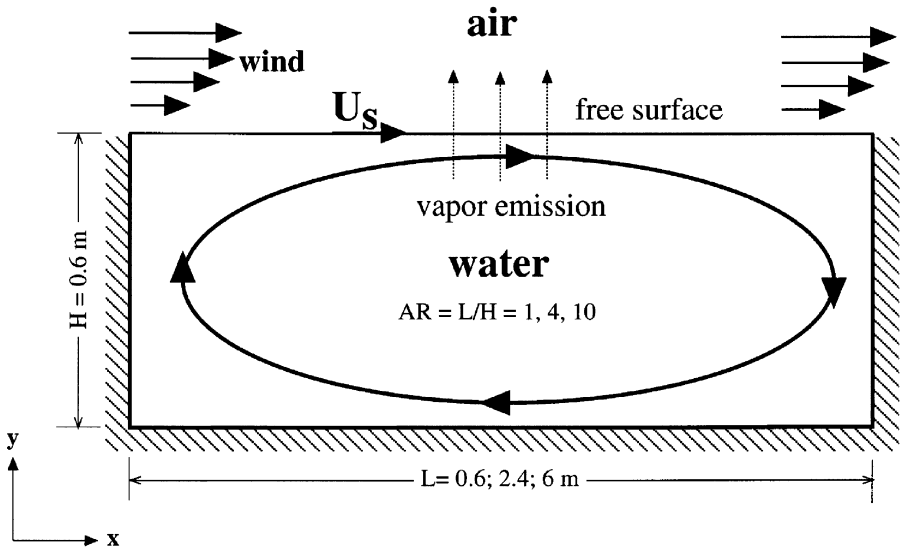

Fig. 1. Schematic of the rectangular pond.

interface concentrations, respectively, at any time t, and y is the distance from the interface. For chemicals with a high Henry's law constant, $C_{wb} \rangle\rangle C_{wi}$ and $(C_{wb} - C_{wi}) \approx C_{wb}$ equation (4) becomes

$$k_L(x) = -\frac{D}{C_b}\left.\frac{\partial C}{\partial y}\right|_x \tag{5}$$

Finally, a surface-average value for the liquid-side mass transfer coefficient is given by

$$\bar{k_L} = \frac{1}{L}\int_0^L k_L(x)\,\mathrm{d}(x) \tag{6}$$

3. Numerical procedure

Numerical solutions of the above governing equations were obtained for the primitive variables by using a two-dimensional version of the computer solver 3DINAMICS [23, 24]. Equations (2) and (3) were discretized following a control volume approach. A non-uniform staggered grid was used, where all scalar magnitudes were located at the center of the computational volume cells, while the velocity components were defined at the respective faces normal to the x and y directions. A second order accurate QUICK scheme (Quadratic Upstream Interpolation for Convective Kinematics) was used for the convective transport terms. This scheme encompasses both accuracy and numerical stability [25, 26].

The main problem when solving the equations in the primitive variable form is the coupling between the velocity and the pressure field. To compute the pressure field the SMAC algorithm was adapted [27]. The time integration involves two steps. At the step from t^n to t^* the approximately velocity field u_i^*, is obtained using the discretized form of equation (2) and the old (time **n**) pressure field as the guessed pressure field. The second step, which updates $\mathbf{u}_i^*$ to $\mathbf{u}_i^{n+1}$, corresponds to the velocity and pressure corrections accomplished by solving the Poisson equation. A critical step in the pressure algorithm, that affects the global efficiency of the code, is the resolution of the Poisson equation. For this purpose, 3DINAMICS makes use of the Conjugate Gradient Method [28] which is faster than other iterative procedures for Poisson-like equations written in the finite difference form.

A steady-state criterion for the dynamic field is imposed in the calculations as given below

$$\frac{\|\mathbf{u}_i^{t+\Delta t} - \mathbf{u}_i^t\|}{\|\mathbf{u}_i^{t+\Delta t}\|} \leqslant 10^{-5} \tag{7}$$

Once the steady-state dynamic field is obtained, the uncoupled mass-transfer equation (3) is solved. Based on the simulation results, both the local and the surface-average interface mass transfer coefficients, defined by equations (5) and (6) can be obtained.

Cuesta et al. [24] validated 3DINAMICS describing the flow in a cubical cavity driven either by the upper moving lid or by the simultaneous heating and cooling of two opposite vertical walls. Pallarés et al. [29] validated 3DINAMICS with the Rayleigh–Benard problem at moderate Rayleigh numbers. The performance of 3DINAMICS in the pond problem was established by a systematic grid-independence study. This study was conducted for a pond geometry with aspect-ratio 4, and for the highest Re_H and Sc numbers covered in the present work, i.e., for $Re_H = 1{,}620$ and $Sc = 2{,}020$. Starting with a coarse grid of 81×81 control volumes, the grid was successively refined to 81×111, 81×151, 81×191, 81×211 and 81×271 with non-uniformly distributed nodes. Figure 2 shows the evolution of the predicted surface-averaged $\bar{K}_L$ value with the number of grid points used. Numerical calculations show that refining the grid in the vertical direction from 211 to 271 nodes results in less than 2% improvement in the calculated value of the surface-averaged liquid-side mass transfer coefficient. Another illustration of the grid selection is provided in Fig. 3 in which the concentration profiles were plotted at the time when the average concentration in the pond declined to half the initial value. The steep change observed in the concentration profiles in Fig. 3 near the interface ($H \approx 0.6$) justified the need for a non-uniform grid distribution. Finally, the concentration profiles, shown in Fig. 3 when a minimum of 5 nodes placed inside the boundary layer when at least 221 nodes are used, support the selection of 81×211 grid to accurately capture the liquid-side concentration boundary layer.

4. Results and discussion

The present study deals with the transfer of pollutants between an impoundment of contaminated water and the surrounding air when weak but steady water phase circulation is induced by wind stress on the water surface. The main goal is to establish the importance of non-uniformities in the distribution of the local liquid-side mass transfer coefficient and evaluate the range of applicability of the penetration theory to predict the corresponding surface-averaged values. Numerical simulations were carried out for three different surface velocities, 3×10^{-5}, 3×10^{-4} and 3×10^{-3} m s^{-1} (corresponding to $Re_H = 16$, 162, 1620), and three different aspect ratios, $AR = 1$, 4, 10. The range of Schmidt numbers considered, $667 \leqslant Sc \leqslant 2020$, encompasses the values corresponding to methanol ($Sc = 667$), benzene ($Sc = 1111$) and pentachlorophenol ($Sc = 2020$).

Figures 4 and 5 show the different flow patterns that are generated in ponds with $AR = 1$ and 4, respectively, at $Re_H = 16$, 162 and 1620. The dynamic fields for $AR = 10$ are not included because they are qualitatively similar to those for $AR = 4$ shown in Fig. 5. At the lowest

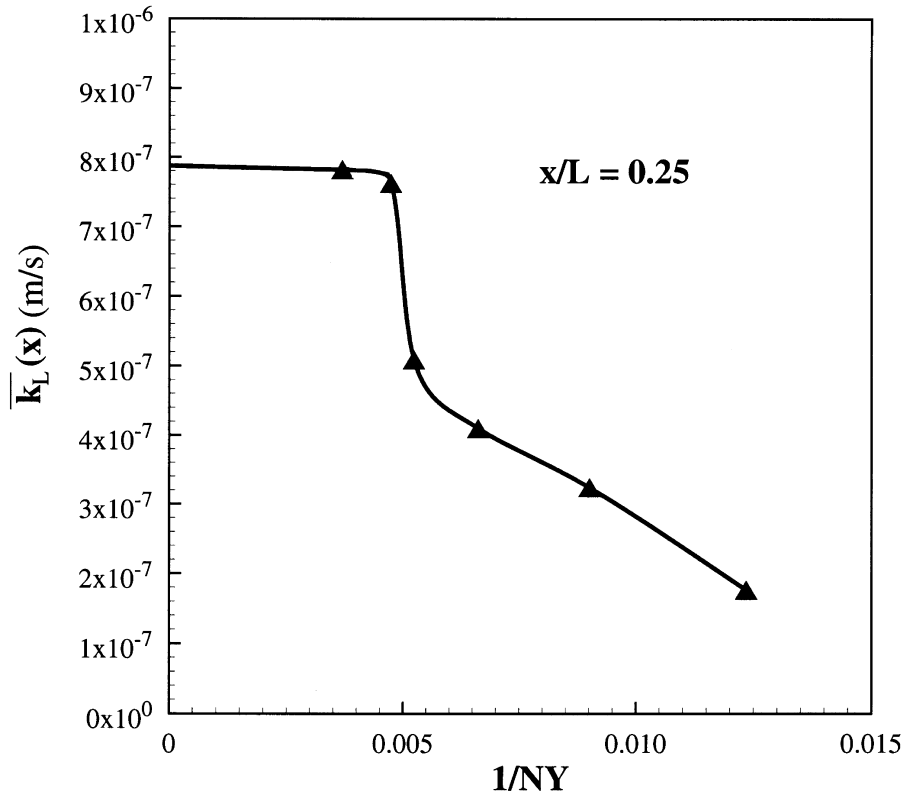

Fig. 2. Surface-averaged mass transfer coefficient for $AR = 4$, $Sc = 2020$ and $Re_H = 620$ as a function of the inverse number of vertical grid nodes (NY).

Reynolds number studied ($Re = 16$) a single recirculating eddy, centered in the geometrical center of the pond, develops for any of the rectangular geometries considered. When the Reynolds number increases this main eddy becomes asymmetric and its center moves closer to the downwind wall. Figures 4 and 5 clearly illustrate that this effect is more pronounced for cavities with $AR > 1$. At the highest $Re_H = 1620$ studied, Figs 4c and 5c, this recirculating motion becomes nearly circular and, thus, an eddy of equal size is observed for any of the three ponds considered. Figure 4c shows that in the square cavity different secondary eddies are formed at the corners, while for $AR > 1$ Fig. 5c shows that a second counterclockwise eddy forms at the upwind region. It is noted that the features of the flow fields obtained for the present simulations are in agreement with those published in the literature [15, 17–19].

The velocity fields depicted in Figs 4 and 5 indicate that the velocity gradients near the interface change significantly with the streamwise direction. As a consequence, the corresponding concentration fields should also change significantly with depth and the streamwise coordinate, as observed already in Fig. 3 for the near-interface region. According to these concentration profiles for the $AR = 4$ pond, mass transfer rates are significantly higher at the entrance upwind region decreasing thereafter, as expected. It is also worth noting that the concentration isolines, as demonstrated in Fig. 6, closely match the streamlines of Fig. 5 because chemicals at high Sc numbers act nearly as passive markers due to their low molecular mass diffusivity in water.

The observation of the concentration profiles near the free-surface at different streamwise locations allows the determination of the thickness of the concentration boundary layer (δ_c). For example, for $Sc = 2020$, $Re_H = 1620$ and $AR = 4$, $\delta_c = 2$ mm at $x = 0.1$ m. The maximum value of δ_c corresponds to the smallest Schmidt number and aspect ratio, i.e., the volatilization for the lowest Sc number studied ($Sc = 667$, i.e., methanol) in the $AR = 10$ pond. Even for $Sc = 667$ the resistance to mass transfer is mainly in a very thin region adjacent to the interface and it is only very weakly affected by the specific flow pattern that develops inside the cavity. This is clearly illustrated in Fig. 7, where the distribution of the local mass transfer coefficient, k_L, along the surface for a given Reynolds and Schmidt numbers, follows the same trend for all ponds. The noticeable feature in Fig. 7 is the varied extent of evolution of k_L, with the x-

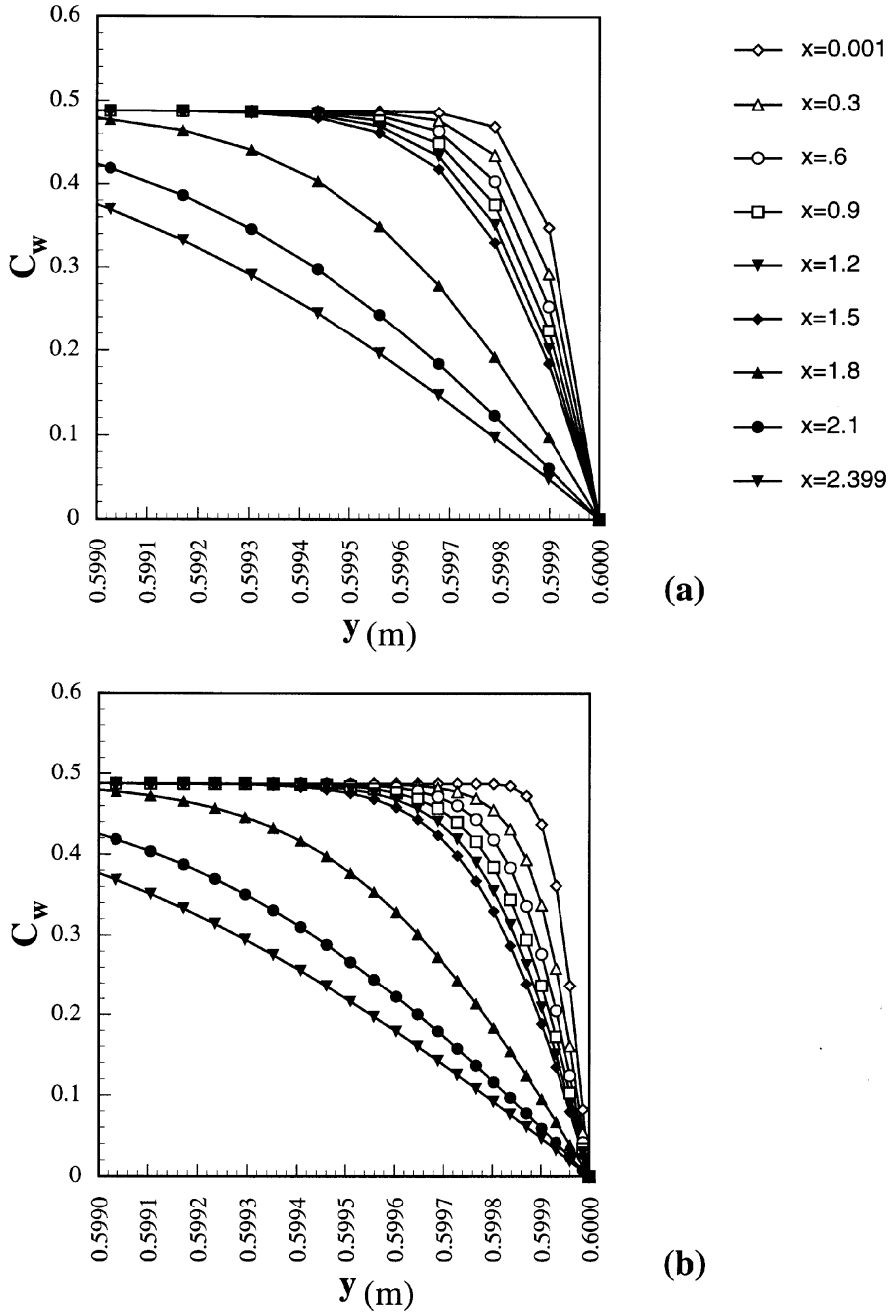

Fig. 3. Dimensionless concentration profiles (C/C_o) at the surface region for $AR = 4$, $Sc = 2020$ and $Re_H = 1620$ at streamwise locations (from top to bottom) $x = 0.001$, 0.3, 0.6, 0.9, 1.2, 1.5, 1.8, 2.1 and 2.399 m, for grids with (a) 211 and (b) 271 nodes. (Note: the profile is plotted at $t \cong 200$ h, when the average concentration reached half the initial value).

direction, imposed by the pond aspect ratio. The same coincidence was found for the other flow and transfer conditions studied. As a consequence, the overall mass transfer rates should be higher for lower aspect ratio ponds. It should be noted that both the local and the surface-averaged liquid-side mass transfer coefficients calculated numerically quickly reach their state-state values, typically after about 3 h of real time.

The variation of the local mass transfer coefficient with Re_H is presented in Fig. 8 for $AR = 4$ and $Sc = 2020$.

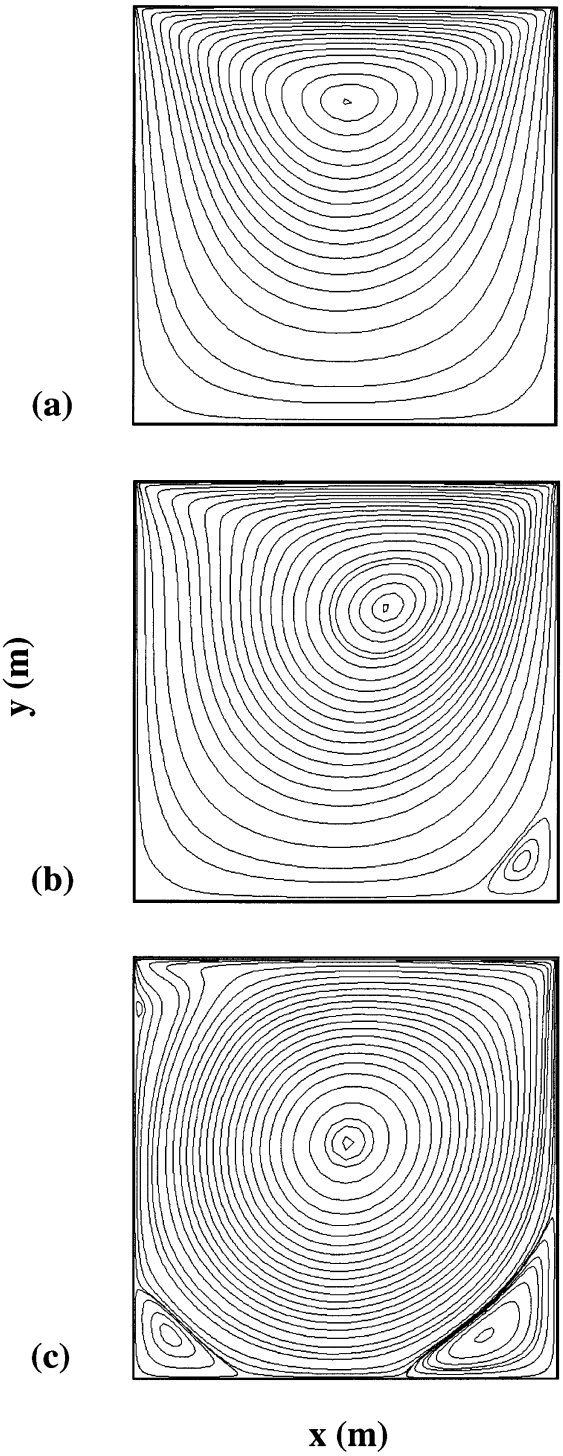

Fig. 4. Streamlines for pond of $AR = 1$ at Re_H: (a) 16, (b) 162 and (c) 1620.

This figure shows that even at low Reynolds numbers the local mass transfer coefficient k_L decreases sharply from the edge of the pond. Again, according to the development of the concentration boundary layer which limits the mass transfer process, the region with higher k_L values extends further down stream as the Reynolds number increases. Both Figs 7 and 8 show that the distribution of the local k_L is not influenced by the presence of different recirculating motions that develop within the pond. Local k_L values also increase with the Sc number and are independent of the flow structures even for a Schmidt number as low as 100 (Fig. 9). This influence would become apparent for concentration boundary layer thickness comparable to the dynamic one, i.e., for $Sc \approx 1$, a situation which would not match realistic volatilization conditions for organic pollutants. The above results suggest that mass transfer theories such as the penetration theory could yield reasonable predictions of the surface-averaged liquid-side mass transfer coefficient for ponds with small aspect ratios and at high Reynolds numbers.

The application of the penetration theory [14, 30] to the mass transfer process in a pond of length L, with a water surface velocity U_s, leads to an expression for the surface-averaged liquid-side mass transfer coefficient of the form

$$k_L = 2\sqrt{\frac{DU_s}{\pi L}} \tag{8}$$

When equation (8) is written in terms of non-dimensional variables, the following expression is obtained

$$Sh_L = \frac{2}{\sqrt{\pi}} Sc^{1/2} Re_L^{1/2} \tag{9}$$

Since $L = AR \cdot H$, equation (9) can be written as

$$Sh_L = \frac{2}{\sqrt{\pi}} AR^{1/2} Sc^{1/2} Re_H^{1/2} \tag{10}$$

where the effect of geometry is included explicitly in the parameter AR.

Equation (10) is plotted in Fig. 10 along with the computed dimensionless mass transfer coefficients (i.e. Sh_L) for all the cases studied here. Several conclusions can be drawn from this figure. First, the calculated Sherwood numbers vary with the expected 0.5 power of the Schmidt number, in agreement with equation (10). Second, the present results and the penetration theory progressively coincide as Re_H increases and, for low Re the agreement is better as AR decreases. While there is fairly good agreement at $Re_H > 1000$ for all AR and Sc covered, the simple penetration model deviates by up to about 50% at low Reynolds numbers and for $AR = 10$.

The deviation of the penetration model from the present numerical calculations (Fig. 10) arises from the fact that the penetration theory assumes short contact times between phases, i.e., a constant concentration in the water side far from the surface. This condition is not

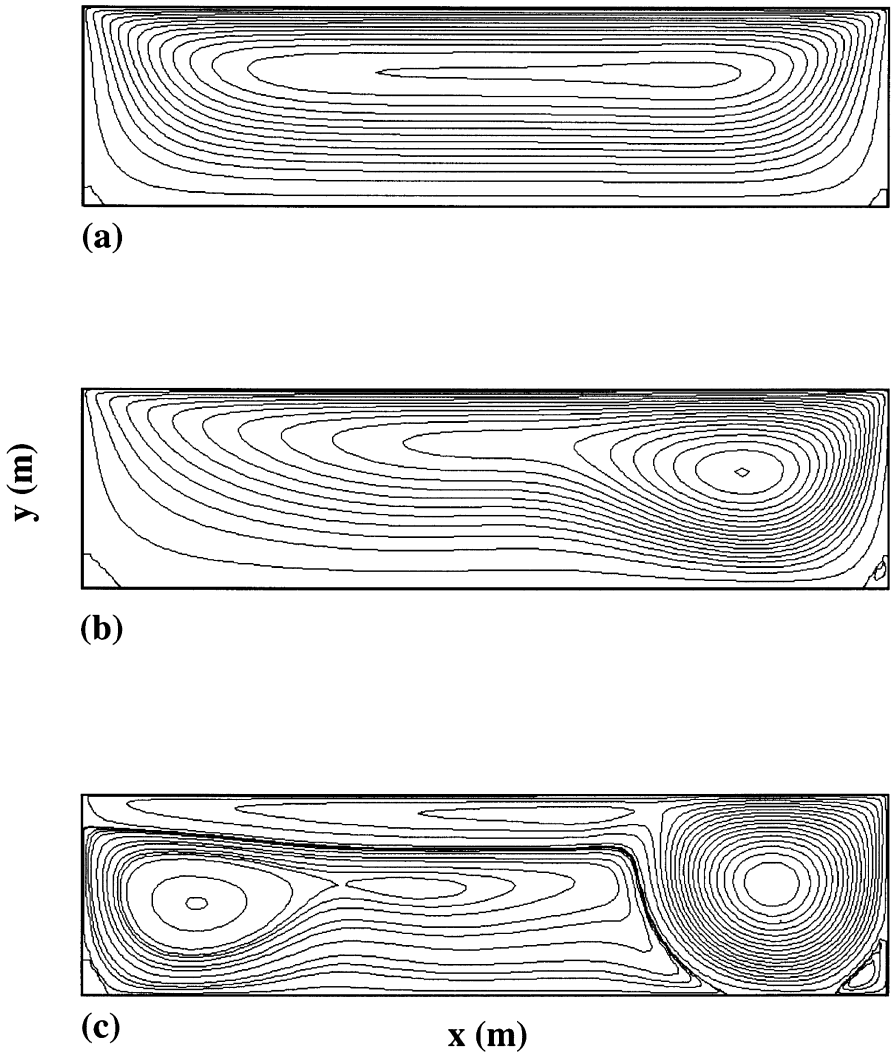

Fig. 5. Streamlines for pond of $AR = 4$ at Re_H: (a) 16, (b) 162 and (c) 1620.

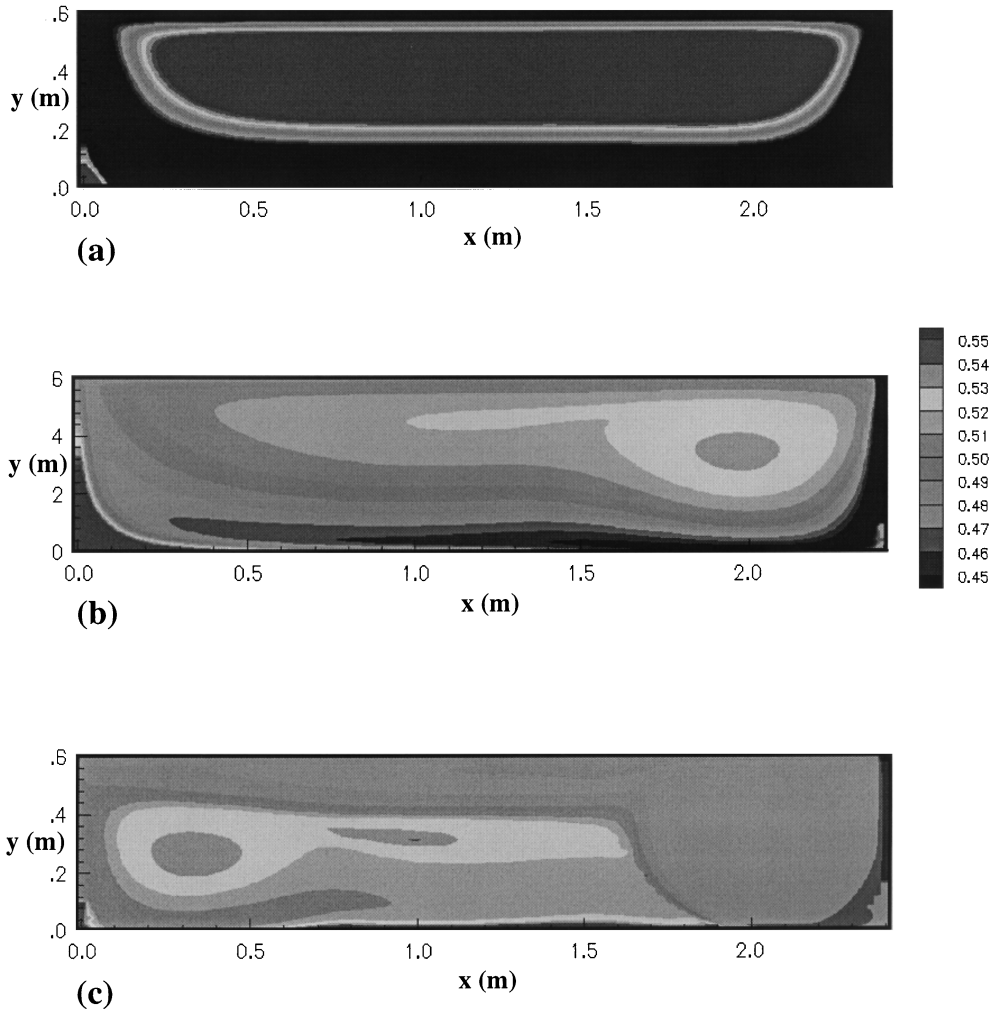

Fig. 6. Concentration isolines ($AR = 4$, $Sc = 2020$) at Re_H: (a) 16, (b) 162 and (c) 1620.

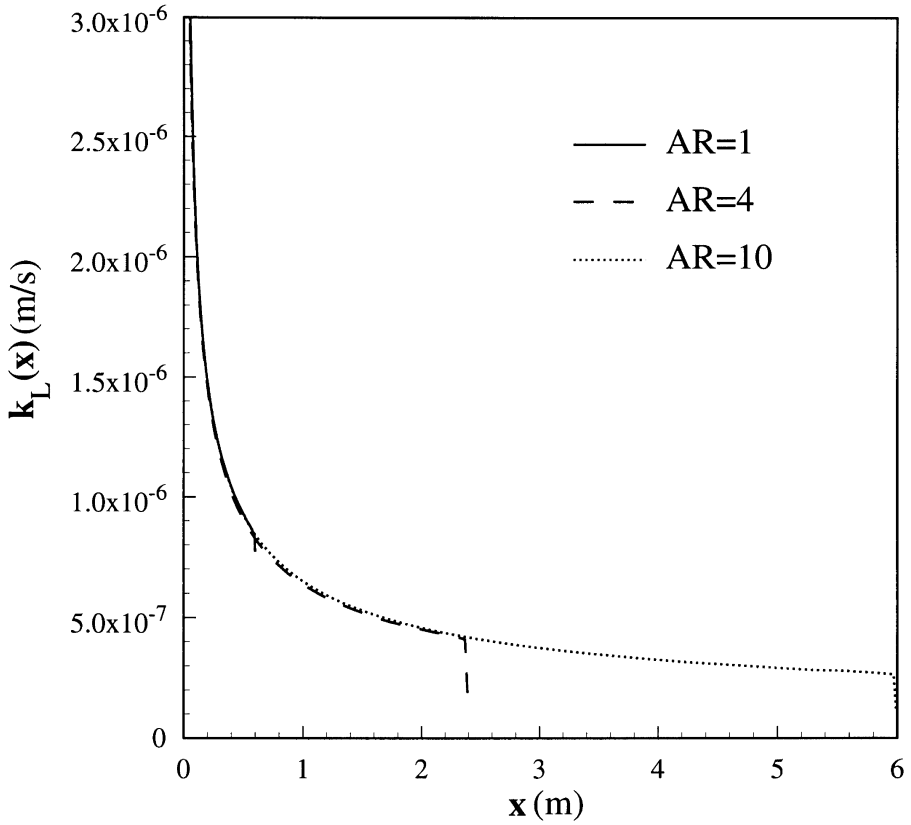

Fig. 7. Variation of the local mass transfer coefficient with streamwise position for $AR = 1, 4, 10$ ($Sc = 2020$, $Re_H = 1620$).

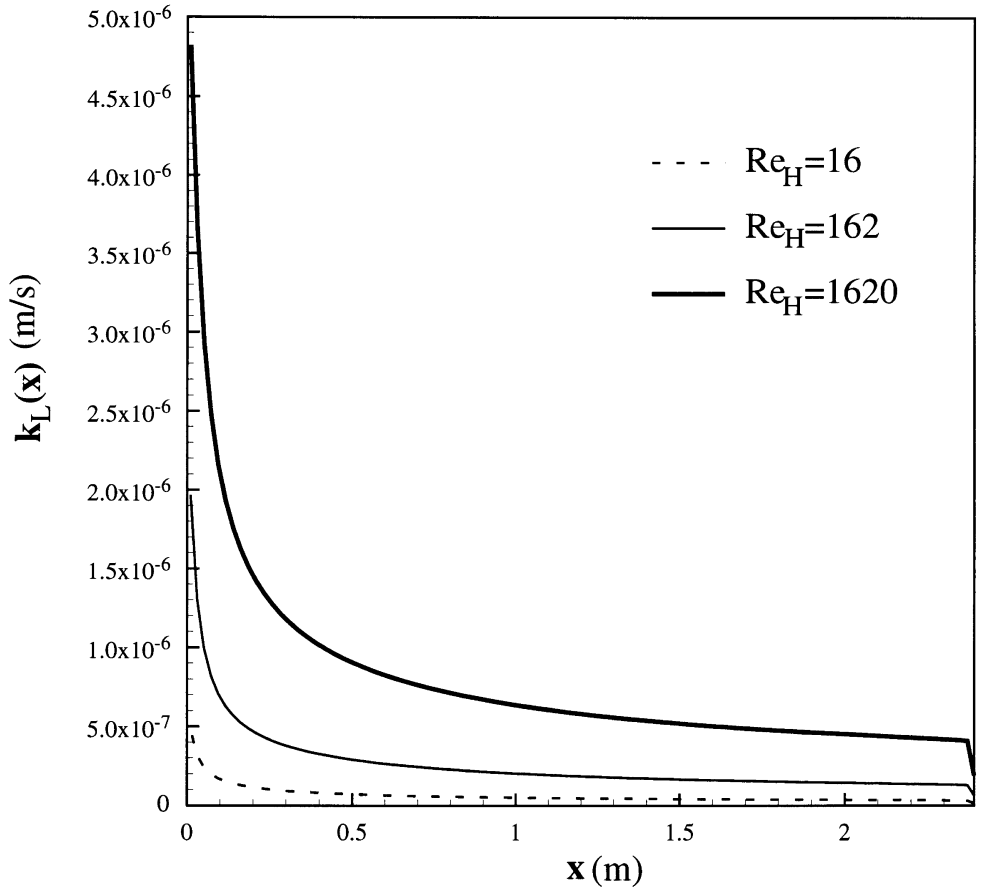

Fig. 8. Variation of the local mass transfer coefficient with streamwise position for $AR = 4$ and $Sc = 2020$ at different Re_H numbers.

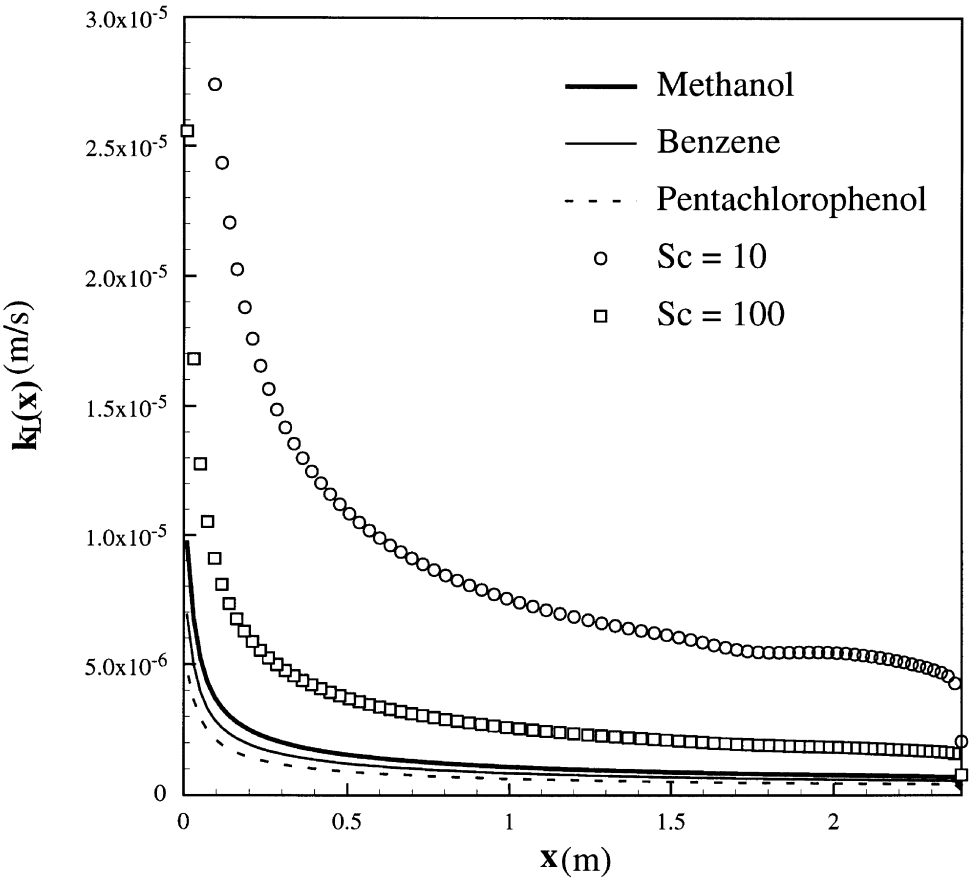

Fig. 9. Effect of the Schmidt number on the local mass transfer coefficient for $AR = 4$ and $Re_H = 1620$.

fulfilled for low surface velocities and geometries with large aspect ratios. The combined effects of low velocities and large AR values can be quantified by correlating the numerical results as given by the following expression

$$Sh_L = \frac{2}{\sqrt{\pi}}\left(1-0.35\left(\frac{AR}{Re_H}\right)^{1/3}\right)AR^{1/2}Sc^{1/2}Re_H^{1/2} \qquad (11)$$

or, in terms of Re_L,

$$Sh_L = \frac{2}{\sqrt{\pi}}\left(1-0.35\frac{AR^{2/3}}{Re_L^{1/3}}\right)Sc^{1/2}Re_L^{1/2} \qquad (12)$$

which encompass the penetration model given by equations (9) and (10) with the factor in parenthesis on the right hand side of equations (11) and (12) being a correction to this model. It is noted that equations (11) and (12) are valid for laminar non-wavy surface conditions and for the aspect ratio (AR) range of 1–10. Also, since surface waves typically begin at a wind speed of about 3 m s^{-1}, the above correlations should not be applied above $Re_H = 4.8 \times 10^4$.

The correlation expressed by equation (12), along with all computed results and the penetration model are presented in Fig. 11. This figure shows that for Re_L values greater than 1000 the present results and their correlation, equation (12), agree with penetration theory. At lower Re_L and aspect ratios greater than unity, where the penetration theory fails, the proposed correlation can be used to describe the computed results and thus estimate the average k_L for other situations of practical interest.

5. Conclusions

A numerical study of chemical volatilization from a shallow pond under the influence of weak wind-induced water recirculation was studied numerically using a two-

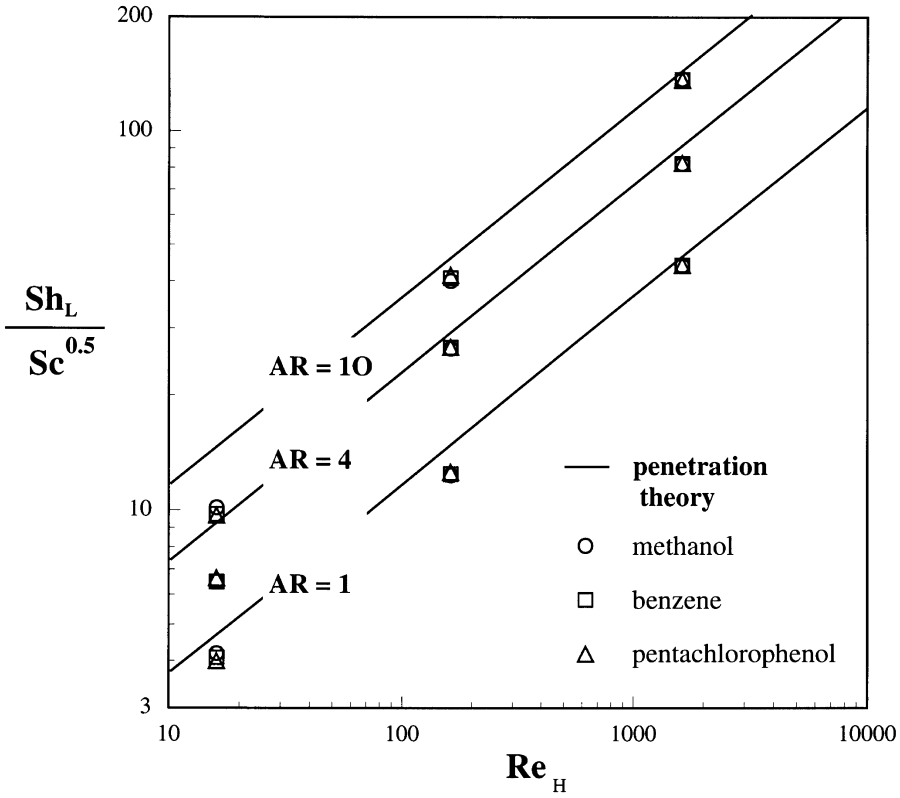

Fig. 10. Comparison of the Sherwood number, Sh_L, determined numerically with the penetration theory for different pond aspect ratios and Reynolds number, Re_H.

dimensional model for fluid flow and mass transfer. The simulation results demonstrate that the water flow field is strongly dependent on both the wind-induced surface velocity (or Reynolds number) and the aspect ratios of the pond. As the Reynolds number (based on pond length) is increased up to 1620, a complex steady flow structure develops consisting of a main recirculating eddy located downwind for aspects ratios greater than unity. At the highest Reynolds number studied the main eddy is of comparable size for all pond aspect ratios.

Both the local and surface-averaged mass transfer coefficients are mainly determined by the flow field in the surface region. This region is essentially independent of the different internal scale motions that develop inside the pond. Under such conditions mass transfer rates calculated from the simple penetration theory, for small pond aspect ratio and high Reynolds numbers, are of sufficient accuracy as confirmed by the present numerical calculations. However, for low Reynolds numbers and especially large pond aspect ratios the penetration theory deviates due to the increased residence time of the fluid elements advected along the surface region. A convenient correlation which extends the penetration theory to include the effect of pond aspect ratio and Reynolds number on residence time was developed based on the present numerical results. Finally, it is noted that the extension of the current study to include the more complex simulation of three-dimensional and non-isothermal circulation in shallow ponds is the subject of an ongoing study.

Acknowledgements

The authors would like to express their gratitude to Cray Research Inc. for providing the supercomputer CPU time needed. The financial support received from DGICY, projects PB93-0656-CO2-01 and PB96-1011, is also gratefully acknowledged. Support received from the Del Amo Foundation, the Center for Catalan Studies and the University of California Toxic Substances Research and Teaching program is also appreciated.

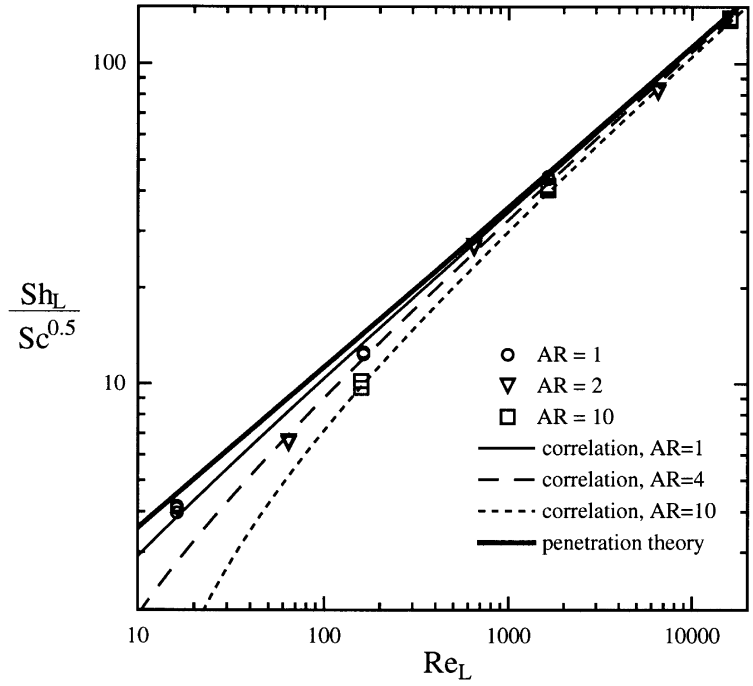

Fig. 11. Sherwood number correlation (Equation (12)) for the surface area-averaged liquid-side mass transfer coefficient.

References

[1] Y. Cohen, in: Y Cohen (editor); Pollutants in a Multimedia Environment, Plenum Press, 7–48, 1986.
[2] C.S. Wilhelm, J.S. Gulliver, (Eds). Air–Water Mass Transfer; Am. Soc. of Civil Eng., New York, 1991.
[3] L.J. Thibodeaux, Chemodynamics. 2nd ed. New York: John Wiley and Sons, 1995.
[4] W.K. Lewis, W.G. Whitman, Principles of gas absorption, Ind. Engng. Chem. 16 (1924) 1215–1220.
[5] J. Peng, J.K. Bewtra, N. Biswas, Volatilization of selected organic compounds from quiescent water, J. Environ. Eng.—ASCE 120 (1994) 662–669.
[6] Y. Cohen, P.A. Ryan, Mass transfer across wind-sheared interfaces, Int. Comm. Heat Mass Transfer 12 (1985) 139–148.
[7] M. Rashidi, G. Hestroni, S. Banerjee, Mechanisms of heat and mass transport at gas–liquid interfaces, Int. J. Heat Mass Transfer 34 (1991) 1799–1810.
[8] S. Kumori, R. Nagaosa, Y. Murkakami, Turbulence structure and mass transfer across a sheared air–water interface in wind-driven turbulence, J. Fluid Mech. 249 (1993) 161–183.
[9] Y. Cohen, W. Cocchio, D. Mackay, Laboratory study of liquid-phase controlled volatilization rates in presence of wind waves, Environ. Sci. Technol. 12 (1978) 553–558.
[10] D. Macky, A.T.K. Yeun, Mass transfer coefficient correlations of volatilization of organic solutes from water, Enviro. Sci. Technol. 17 (1983) 211–217.
[11] W.J. Lyman, W.F. Reehl, D.H. Rosenblatt, Handbook of Chemical Property Estimation Methods. American Chemical Society, Washington DC, 1990.
[12] P. Danckewerts, Gas–liquid Reactions. McGraw-Hill, New York, 1970.
[13] W.E. Asher, J.F. Pankow, Prediction of gas/water mass transport coefficients by a surface renewal model, Environ. Sci. Technol. 25 (1991) 1294–1300.
[14] R.B. Bird, W.E. Stewart, E.N. Lightfoot, Transport Phenomena, 2nd ed., John Wiley and Sons, New York, 1960.
[15] J.A.T. Bye, Numerical solutions of the steady-state vorticity equation in rectangular basins, J. Fluid Mech. 26 (1966) 577–598.
[16] V. O'Brien, Closed streamlines associated with channel flow over a cavity, Phys. Fluids, 15 (1972) 2089–2097.
[17] M.A. Kumagai, A numerical study of wind-driven circulation in rectangular cavities, J. Comp. Physics. 47 (1982) 130–145.
[18] T.B. Gatski, C.E. Grosch, M.E. Rose, A numerical study of the two-dimensional Navier–Stokes equations in vorticity–velocity variables, J. Comp. Physics 48 (1982) 1–22.
[19] M.D. Neary, K.D. Stephanoff, Shear-layer-driven transition in a rectangular cavity, Phys. Fluids 30 (1987) 2936–2946.
[20] H.N. Chang, H.W. Ruy, D.H. Park, Y.S. Park, Effect of external laminar channel flow on mass transfer in a cavity, Int. J. Heat Mass Transfer 3 (1987) 2137–2149.
[21] L.J. Thibodeaux, B. Becker, Chemical transport rates near the sediment in wastewater impoundements, Environmental Progress 1 (1982) 296–300.

[22] J.P. Benqué, A. Hauguel, P.L. Viollet, Engineering Application of Computational Hydraulics, Vol. II, Pitman Advanced Pub. Program, 1982.
[23] I. Cuesta, Estudi numeric de fluxos laminars i turbulents en una cavitat cubica. PhD thesis, Universitat Rovira i Virgili, Tarragona, Spain, 1993.
[24] I. Cuesta, F.X. Grau, F. Giralt, Simulación numérica de flujos tridimensionales no estacionarios mediante el código de segundo orden 3DINAMICS. Anales de Química 91 (1995) 655–665.
[25] B.P. Leonard, A stable and accurate convective modelling procedure based on quadratic upstream interpolation, Comp. Meth. Appl. Mech. & Eng. 19 (1979) 59–88.
[26] C.-Y. Perng, R.L. Street, Three-dimensional unsteady flow simulations: alternative strategies for a volume-averaged calculation, Int. J. Numerical Methods Fluids 9 (1989) 341–362.
[27] A.A. Amsden, F.H. Harlow, The SMAC methods: a numerical technique for calculating incompressible fluid flows. Technical report, LA-4370, Los Alamos Scientific Laboratory, University of California, 1970.
[28] P.K. Koshla, S.G. Rubin, A conjugate gradient iterative method, Computers and Fluids 9 (1981) 109–121.
[29] J. Pallares, I. Cuesta, F.X. Grau, F. Giralt, Natural convection in a cubical cavity heated from below at low Rayleigh numbers, Int. J. Heat Mass Transfer 39 (1996) 3233–3247.
[30] R. Higbie, The rate of absorption of a pure gas into a still liquid during short periods of exposure, Trans. Am. Inst. Chem. Engrs. 35 (1935) 365–389.